Journal of Zhejiang University-SCIENCE A (Applied Physics & Engineering)
ISSN 1673-565X (Print); ISSN 1862-1775 (Online)
www.jzus.zju.edu.cn; link.springer.com
E-mail: jzus_a@zju.edu.cn

Crack identification in functionally graded material framed structures using stationary wavelet transform and neural network*

Nguyen Tien KHIEM[1], Tran Van LIEN[†‡2], Ngo Trong DUC[3]

[1]*Institute of Mechanics, Vietnam Academy of Science and Technology, Hanoi 10072, Vietnam*

[2]*Faculty of Building and Industrial Construction, National University of Civil Engineering, Hanoi 11600, Vietnam*

[3]*Fujita Corporation, Hanoi 11000, Vietnam*

[†]E-mail: LienTV@nuce.edu.vn

Received Sept. 8, 2020; Revision accepted Dec. 6, 2020; Crosschecked July 30, 2021

Abstract: In this paper, an integrated procedure is proposed to identify cracks in a portal framed structure made of functionally graded material (FGM) using stationary wavelet transform (SWT) and neural network (NN). Material properties of the structure vary along the thickness of beam elements by the power law of volumn distribution. Cracks are assumed to be open and are modeled by double massless springs with stiffness calculated from their depth. The dynamic stiffness method (DSM) is developed to calculate the mode shapes of a cracked frame structure based on shape functions obtained as a general solution of vibration in multiple cracked FGM Timoshenko beams. The SWT of mode shapes is examined for localization of potential cracks in the frame structure and utilized as the input data of NN for crack depth identification. The integrated procedure proposed is shown to be very effective for accurately assessing crack locations and depths in FGM structures, even with noisy measured mode shapes and a limited amount of measured data.

Key words: Crack identification; Functionally graded material (FGM); Neural network (NN); Stationary wavelet transform (SWT); Dynamic stiffness method

https://doi.org/10.1631/jzus.A2000402 **CLC number:** TU43

1 Introduction

The dynamics of basic structures such as beams and plates made of functionally graded material (FGM) have attracted the attention of researches and engineers in many high-tech industries due to its valuable properties (Chakraverty and Pradhan, 2016; Elishakoff et al., 2016). The fundamental results have been attained for perfect FGM structures rather than for damaged ones such as cracked structures. This is, perhaps, because of the greater complexity of the problems in either fracture mechanics of FGM (Jin and Batra, 1996; Erdogan and Wu, 1997; Gu and Asaro, 1997; Pan et al., 2009) or dynamics of cracked FGM structures (Yang and Chen, 2008; Yang et al., 2008; Ke et al., 2009; Wei et al., 2012; Aydin, 2013; Sherafatnia et al., 2013; Khiem et al., 2017) that have variation in both material and geometry. Though the spring model of crack has been used in most of the studies on cracked functionally graded beams, there is no consistent formula for calculating stiffness of the equivalent spring. Furthermore, numerous studies on FGM beams have been formulated using the beam's central surface instead of a neutral one (Eltaher et al., 2013; Larbi et al., 2013). Adopting the central instead of the neutral surface in FGM beams may lead to erroneous results for the beams with material properties varying along their thickness, especially in the

‡ Corresponding author

* Project supported by the Vietnam National Foundation for Science and Technology Development (No. 107.02-2017.301)

ORCID: Tran Van LIE, https://orcid.org/0000-0002-2026-3831; Nguyen Tien KHIEM, https://orcid.org/0000-0001-5195-2704

case of short or thick beams, such as Timoshenko beams, made of FGM. Moreover, taking account of the actual position of the neutral axis in vibration analysis of an FGM Timoshenko beam not only simplifies the governing equations of the beam but also allows a condition for deriving the uncoupling of the axial and flexural vibration modes in FGM beams (Khiem and Huyen, 2016).

Among the various methods proposed for vibration analysis of functionally graded beams with cracks, there are the conventional analytical approach (Yang and Chen, 2008; Yang et al., 2008; Ke et al., 2009; Wei et al., 2012; Aydin, 2013; Sherafatnia et al., 2013; Khiem et al., 2017), Ritz (Kitipornchai et al., 2009) and Galerkin's (Yan et al., 2011) techniques, differential quadrature (Matbuly et al., 2009), and the harmonic balance method (Panigrahi and Pohit, 2018). These techniques enable thorough investigation of the effect of cracks in combination with the material properties of modal parameters of FGM beams and their dynamic response to various loads. Nevertheless, the analytical approaches are limited to use only for 1D structures. The finite element method (FEM), used in (Akbaş, 2013) for analysis and identification of cracked FGM beams, is preferred in applications for more complex structures such as cracked frames. However, by using only static (frequency-independent) shape functions the FEM cannot be employed to capture all the high-frequency vibration modes that are more typical of FGM structures. The so-called dynamic stiffness method (DSM), well-known as the most exact tool for vibration analysis to date, allows examination of the arbitrary high-frequency vibration modes of elastic structures including the FGM ones. This method has been proposed for modal analysis of intact (Su and Banerjee, 2015) and cracked (Lien et al., 2019b) FGM Timoshenko beams, but, to the authors' knowledge, it has not been used for crack identification. Recently, the DSM was developed by Banerjee and Ananthapuvirajah (2018) for modal analysis of an intact portal frame made of FGM, and that work has motivated the authors in the present study to apply that method for a frame with cracks.

The problem of crack identification in FGM structures is receiving increased attention from both structural engineers and researchers. Some procedures have been developed to detect and quantify cracks in structures. Nanthakumar et al. (2016) proposed an algorithm to detect inclusion interfaces in piezoelectric structures based on a level set. Yu and Chu (2009) proposed identifying the location and size of a crack in FGM beam by using the frequency contours method. Eftekhari et al. (2013) and Khiem and Huyen (2017) developed the frequency-based technique to detect a single crack in FGM beams using characteristic equations. Banerjee et al. (2016) demonstrated that combination of so-called response surface methodology with a generic algorithm allowed development of a successful procedure for prediction of crack location and depth in an FGM Timoshenko beam. Nazari and Abolbashari (2013) and Abolbashari et al. (2014) showed that the artificial neural network provides an efficient technique for double and multiple crack identifications in FGM beams. Zhu et al. (2019) proposed a procedure for crack identification in an FGM beam using continuous wavelet transform (CWT) and Lien and Duc (2019) investigated the problem of crack identification based on stationary wavelet transform (SWT) of mode shapes. Recently, Lien et al. (2019a) proposed a method combining neuron network (NN) and SWT of mode shapes and dynamic deflections for crack identification in cracked multi-span FGM beams.

While the latter studies are limited to considering cracked FGM beams, this study is devoted to multiple cracked identification in frames made of FGM using the technique proposed in (Lien et al., 2019a) for multi-span beams. Cracked frame structures were considered in (Khiem, 2006; Caddemi and Caliò, 2013; Caddemi et al., 2018), but they consisted of cracked homogeneous Euler-Bernoulli beam elements. In this paper, first, we establish the dynamic stiffness model of a cracked FGM frame based on an explicit exact solution of free vibration in a multiple cracked FGM beam element. Then, the conducted dynamics stiffness model is employed for calculating mode shapes of a multiple-cracked frame. Next, the calculated mode shapes have been analyzed by using the SWT that allows clear exhibition of crack position in the structure. This provides an efficient tool for crack localization in the FGM frames. To complete the crack identification problem, the wavelet detail coefficients of the frame's mode shapes are put into a properly established NN to estimate the depth of the localized cracks. Thus, an integrated procedure,

proposed in (Lien et al., 2019a) for crack identification in multi-span FGM beams, is developed here for multiple cracked identification of frame structures made of FGM. A case study has been undertaken to illustrate the theoretical development and investigate the influence of measurement noise on results of crack identification by using the integrated procedure.

2 Dynamic stiffness method of modal analysis of multiple cracked FGM frames

2.1 Governing equations

Consider an elastic beam of length L with rectangular cross section width b and height h (Fig. 1) assuming that the material properties vary by the power law distribution (Elishakoff et al., 2016)

$$\begin{Bmatrix} E(z) \\ G(z) \\ \rho(z) \end{Bmatrix} = \begin{Bmatrix} E_\mathrm{b} \\ G_\mathrm{b} \\ \rho_\mathrm{b} \end{Bmatrix} + \begin{Bmatrix} E_\mathrm{t}-E_\mathrm{b} \\ G_\mathrm{t}-G_\mathrm{b} \\ \rho_\mathrm{t}-\rho_\mathrm{b} \end{Bmatrix} \left(\frac{z}{h}+\frac{1}{2}\right)^n, \quad -h/2 \le z \le h/2, \tag{1}$$

where E, G, and ρ stand for Young's modulus, shear modulus, and mass density, respectively; subscripts t and b denote the top and bottom material, respectively; n is the power law exponent; z is the ordinate of a point from the mid plane. According to the Timoshenko beam theory, the displacement field of the beam is expressed as

$$\begin{aligned} u(x,z,t) &= u_0(x,t)-(z-h_0)\theta(x,t), \\ w(x,z,t) &= w_0(x,t), \end{aligned} \tag{2}$$

where $u_0(x, t)$ and $w_0(x, t)$ are the axial and lateral displacements at the point on the neutral plane, respectively, t is the time variable, and x is the spatial variable; θ is the rotation of cross section; h_0 is the distance from the neutral axis to the mid plane (Eltaher et al., 2013).

$$h_0 = \frac{n(r_E-1)h}{2(n+2)(n+r_E)}, \quad r_E = \frac{E_\mathrm{t}}{E_\mathrm{b}}. \tag{3}$$

where r_E is the ratio of Young's modulus of the top material to that of the bottom material.

Using the Hamilton principle, equations of motion for the beam can be derived in the form

$$\begin{aligned} (I_{11}\ddot{u}_0 - A_{11}u_0'') - I_{12}\ddot{\theta} &= 0, \\ I_{12}\ddot{u}_0 - (I_{22}\ddot{\theta} - A_{22}\theta'') + A_{33}(w_0'-\theta) &= 0, \\ I_{11}\ddot{w}_0 - A_{33}(w_0''-\theta') &= 0, \end{aligned} \tag{4}$$

where dot denotes derivative with respect to the time variable t, comma denotes derivative with respect to the spatial variable x, A_{11}, A_{22}, and A_{33} are the rigidities, and I_{11}, I_{12}, and I_{22} are the mass moments.

$$\begin{aligned} (A_{11}, A_{12}, A_{22}) &= \int_A E(z)\left(1, z-h_0, (z-h_0)^2\right)\mathrm{d}A, \\ (I_{11}, I_{12}, I_{22}) &= \int_A \rho(z)\left(1, z-h_0, (z-h_0)^2\right)\mathrm{d}A, \\ A_{33} &= \frac{5}{6}\int_A G(z)\mathrm{d}A, \quad r_\rho = \frac{\rho_\mathrm{t}}{\rho_\mathrm{b}}. \end{aligned} \tag{5}$$

Note that the axial and lateral vibrations in the FGM beam are uncoupled like the homogeneous beam if I_{12}=0 or $(r_E - r_\rho)n = 0$, otherwise, the vibration components in the beam are coupled.

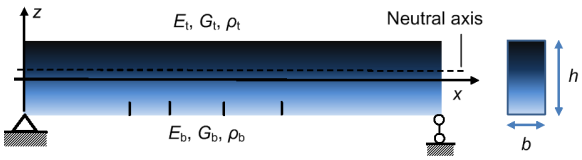

Fig. 1 Model of cracked FGM beam

Introducing the vector:

$$[U, \Theta, W] = \int_{-\infty}^{\infty} \{u_0(x,t), \theta(x,t), w_0(x,t)\}\mathrm{e}^{-\mathrm{i}\omega t}\mathrm{d}t, \tag{6}$$

where U, Θ, and W are respectively the amplitudes of axial displacement, rotation, and deflection, and ω is the frequency of vibration. Eq. (4) are transformed to

$$\boldsymbol{A}\boldsymbol{z}''(x,\omega) + \boldsymbol{\Pi}\boldsymbol{z}'(x,\omega) + \boldsymbol{\Gamma}(\omega)\boldsymbol{z}(x,\omega) = \boldsymbol{0}, \tag{7}$$

where vectors $\boldsymbol{z}=[U, \Theta, W]^\mathrm{T}$, $\boldsymbol{z}''=\mathrm{d}^2\boldsymbol{z}/\mathrm{d}x^2$, and matrices

$$\boldsymbol{A}=\begin{bmatrix} A_{11} & 0 & 0 \\ 0 & A_{22} & 0 \\ 0 & 0 & A_{33} \end{bmatrix},\quad \boldsymbol{\Pi}=\begin{bmatrix} 0 & 0 & 0 \\ 0 & 0 & A_{33} \\ 0 & -A_{33} & 0 \end{bmatrix},$$

$$\boldsymbol{\Gamma}(\omega)=\begin{bmatrix} \omega^2 I_{11} & -\omega^2 I_{12} & 0 \\ -\omega^2 I_{12} & \omega^2 I_{22}-A_{33} & 0 \\ 0 & 0 & \omega^2 I_{11} \end{bmatrix}.$$

Obviously, the general solution of the ordinary differential equation (Eq. (7)) can be expressed as

$$\boldsymbol{z}_0(x,\omega)=\boldsymbol{G}_0(x,\omega)\boldsymbol{C}, \tag{8}$$

where $\boldsymbol{C}=[C_1, C_2, \ldots, C_6]^{\mathrm{T}}$ is a constant vector, $\boldsymbol{G}_0(x,\omega)$ is the function matrix (Lien et al., 2019b), which is given by

$$\boldsymbol{G}_0(x,\omega)=\begin{bmatrix} \alpha_1 \mathrm{e}^{k_1 x} & \alpha_2 \mathrm{e}^{k_2 x} & \alpha_3 \mathrm{e}^{k_3 x} & \alpha_1 \mathrm{e}^{-k_1 x} & \alpha_2 \mathrm{e}^{-k_2 x} & \alpha_3 \mathrm{e}^{-k_3 x} \\ \mathrm{e}^{k_1 x} & \mathrm{e}^{k_2 x} & \mathrm{e}^{k_3 x} & \mathrm{e}^{-k_1 x} & \mathrm{e}^{-k_2 x} & \mathrm{e}^{-k_3 x} \\ \beta_1 \mathrm{e}^{k_1 x} & \beta_2 \mathrm{e}^{k_2 x} & \beta_3 \mathrm{e}^{k_3 x} & -\beta_1 \mathrm{e}^{-k_1 x} & -\beta_2 \mathrm{e}^{-k_2 x} & -\beta_3 \mathrm{e}^{-k_3 x} \end{bmatrix},$$

$$\alpha_j=\frac{\omega^2 I_{12}}{\omega^2 I_{11}+k_j^2 A_{11}},\ \beta_j=\frac{k_j A_{33}}{(\omega^2 I_{11}+k_j^2 A_{33})},\ j=1,2,3, \tag{9}$$

with wave numbers k_1, k_2, k_3 sought from the characteristic equation $\det[\lambda^2\boldsymbol{A}+\lambda\boldsymbol{\Pi}+\boldsymbol{\Gamma}]=0$. α_j and β_j are respectively the amplitudes of axial displacement and deflection related to the wave number k_j.

It is supposed that the beam has been cracked at position e_j and the crack is modeled by two springs, an axial spring of stiffness T and a rotational spring of stiffness R as shown in Fig. 2. Therefore, the continuous conditions at the cracks are (Jin and Batra, 1996; Banerjee et al., 2016):

$$\begin{aligned} U(e_j+0)&=U(e_j-0)+\gamma_{aj}U_x'(e_j), \\ \Theta(e_j+0)&=\Theta(e_j-0)+\gamma_{bj}\Theta_x(e_j), \\ W(e_j+0)&=W(e_j-0), \\ U_x'(e_j+0)&=U_x'(e_j-0), \\ \Theta_x'(e_j+0)&=\Theta_x'(e_j-0), \\ W_x'(e_j+0)&=W_x'(e_j-0)+\gamma_{bj}\Theta_x'(e_j). \end{aligned} \tag{10}$$

The magnitudes γ_{aj}, γ_{bj} are calculated from the crack depth a_j (Khiem et al., 2017).

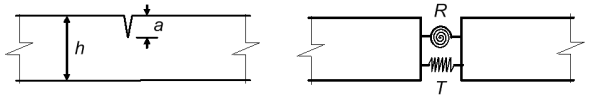

Fig. 2 Model of two equivalent springs

Obviously, the solution Eq. (8) of Eq. (7) is continuous along the whole beam length and it is a general solution of free vibration in uncracked FGM beam. However, the solution satisfying additionally conditions Eq. (10) and acknowledged as general solution for free vibration in multiple cracked FGM beam can be represented as (Lien and Duc, 2019)

$$\boldsymbol{z}(x,\omega)=\boldsymbol{\Phi}(x,\omega)\cdot\boldsymbol{C}, \tag{11}$$

where

$$\boldsymbol{\Phi}(x,\omega)=\boldsymbol{G}_0(x,\omega)+\sum_{j=1}^{n}\boldsymbol{K}(x-e_j,\gamma_{aj},\gamma_{bj})\cdot\boldsymbol{\Omega}_j,$$

$$\boldsymbol{K}(x,\gamma_a,\gamma_b)=\begin{cases}\boldsymbol{G}(x,\gamma_a,\gamma_b), & x>0,\\ \boldsymbol{0}, & x\le 0,\end{cases}$$

$$\boldsymbol{K}'(x,\gamma_a,\gamma_b)=\begin{cases}\boldsymbol{G}'(x,\gamma_a,\gamma_b), & x>0,\\ \boldsymbol{0}, & x\le 0,\end{cases}$$

$$\boldsymbol{G}(x,\gamma_a,\gamma_b)=\begin{bmatrix} \gamma_a\sum_{i=1}^{3}\alpha_i\delta_{i1}\cosh(k_i x) & \gamma_b\sum_{i=1}^{3}\alpha_i(\delta_{i2}+\delta_{i3})\cosh(k_i x) & 0 \\ \gamma_a\sum_{i=1}^{3}\delta_{i1}\cosh(k_i x) & \gamma_b\sum_{i=1}^{3}(\delta_{i2}+\delta_{i3})\cosh(k_i x) & 0 \\ \gamma_a\sum_{i=1}^{3}\beta_i\delta_{i1}\sinh(k_i x) & \gamma_b\sum_{i=1}^{3}\beta_i(\delta_{i2}+\delta_{i3})\sinh(k_i x) & 0 \end{bmatrix}, \tag{12}$$

where

$$\begin{aligned} &\delta_{11}=(k_3\beta_3-k_2\beta_2)/\Delta,\ \delta_{12}=(\alpha_3 k_2\beta_2-\alpha_2 k_3\beta_3)/\Delta, \\ &\delta_{13}=(\alpha_2-\alpha_3)/\Delta,\ \delta_{21}=(k_1\beta_1-k_3\beta_3)/\Delta, \\ &\delta_{22}=(\alpha_1 k_3\beta_3-\alpha_3 k_1\beta_1)/\Delta,\ \delta_{23}=(\alpha_3-\alpha_1)/\Delta, \\ &\delta_{31}=(k_2\beta_2-k_1\beta_1)/\Delta,\ \delta_{32}=(\alpha_2 k_1\beta_1-\alpha_1 k_2\beta_2)/\Delta, \\ &\delta_{33}=(\alpha_1-\alpha_2)/\Delta, \\ &\Delta=k_1\beta_1(\alpha_2-\alpha_3)+k_2\beta_2(\alpha_3-\alpha_1)+k_3\beta_3(\alpha_1-\alpha_2). \end{aligned}$$

The 3×6 matrices $\boldsymbol{\Omega}_j$ introduced in Eq. (12) are determined from the recurrent relationship

$$\boldsymbol{\Omega}_j=\boldsymbol{G}_0'(e_j,\omega)+\sum_{k=1}^{j-1}\boldsymbol{G}'(e_j-e_k,\gamma_{ak},\gamma_{bk})\cdot\boldsymbol{\Omega}_k. \tag{13}$$

2.2 Dynamic stiffness matrix for the cracked FGM Timoshenko beam element

The nodal displacement $\boldsymbol{U}_e$ and force vector $\boldsymbol{P}_e$ of a multiple cracked Timoshenko beam element (Fig. 3) are given by (Lien et al., 2019b)

$$\begin{aligned}\boldsymbol{U}_e(\omega)&=[U_1,\Theta_1,W_1,U_2,\Theta_2,W_2]^{\mathrm{T}},\\ \boldsymbol{P}_e(\omega)&=[N_1,M_1,Q_1,N_2,M_2,Q_2]^{\mathrm{T}},\end{aligned}\tag{14}$$

where

$$\begin{aligned}&N_1=-\left(A_{11}\partial_x z_1\right)_{x=0},\ M_1=-\left(A_{22}\partial_x z_2\right)_{x=0},\\ &Q_1=-A_{33}\left(\partial_x z_3-z_2\right)_{x=0},\ N_2=\left(A_{11}\partial_x z_1\right)_{x=L},\\ &M_2=\left(A_{22}\partial_x z_2\right)_{x=L},\ Q_2=A_{33}\left(\partial_x z_3-z_2\right)_{x=L}.\end{aligned}$$

Rewriting the equations in matrix form, we can obtain:

$$\begin{aligned}[U_1,\Theta_1,W_1]^{\mathrm{T}}&=\boldsymbol{z}(0,\omega),\\ [U_2,\Theta_2,W_2]^{\mathrm{T}}&=\boldsymbol{z}(L,\omega),\\ [N_1,M_1,Q_1]^{\mathrm{T}}&=\boldsymbol{\mathfrak{R}}\boldsymbol{z}(x,\omega)_{x=0},\\ [N_2,M_2,Q_2]^{\mathrm{T}}&=\boldsymbol{\mathfrak{R}}\boldsymbol{z}(x,\omega)_{x=L},\end{aligned}\tag{15}$$

where $\boldsymbol{\mathfrak{R}}$ is the differential operator:

$$\boldsymbol{\mathfrak{R}}=\begin{bmatrix}A_{11}\partial_x & 0 & 0\\ 0 & A_{22}\partial_x & 0\\ 0 & -A_{33} & A_{33}\partial_x\end{bmatrix}.$$

Substituting Eq. (11) into Eq. (15) yields

$$\begin{aligned}[N_1,M_1,Q_1]^{\mathrm{T}}&=\boldsymbol{\mathfrak{R}}\boldsymbol{\Phi}(x,\omega)_{x=0}\boldsymbol{C},\\ [N_2,M_2,Q_2]^{\mathrm{T}}&=\boldsymbol{\mathfrak{R}}\boldsymbol{\Phi}(x,\omega)_{x=L}\boldsymbol{C},\end{aligned}$$

or

$$\boldsymbol{U}_e=\begin{bmatrix}\boldsymbol{\Phi}(0,\omega)\\ \boldsymbol{\Phi}(L,\omega)\end{bmatrix}\boldsymbol{C},\quad \boldsymbol{P}_e=\begin{bmatrix}\boldsymbol{\mathfrak{R}}\boldsymbol{\Phi}(x,\omega)_{x=0}\\ \boldsymbol{\mathfrak{R}}\boldsymbol{\Phi}(x,\omega)_{x=L}\end{bmatrix}\boldsymbol{C}.\tag{16}$$

Eliminating vector $\boldsymbol{C}$ from Eq. (16) leads to

$$\boldsymbol{P}_e=\boldsymbol{D}_e(\omega)\boldsymbol{U}_e,\tag{17}$$

where the matrix

$$\boldsymbol{D}_e(\omega)=\begin{bmatrix}\boldsymbol{\mathfrak{R}}\boldsymbol{\Phi}(x,\omega)_{x=0}\\ \boldsymbol{\mathfrak{R}}\boldsymbol{\Phi}(x,\omega)_{x=L}\end{bmatrix}\cdot\begin{bmatrix}\boldsymbol{\Phi}(0,\omega)\\ \boldsymbol{\Phi}(0,\omega)\end{bmatrix}^{-1}\tag{18}$$

is the dynamic stiffness matrix for the FGM Timoshenko beam element.

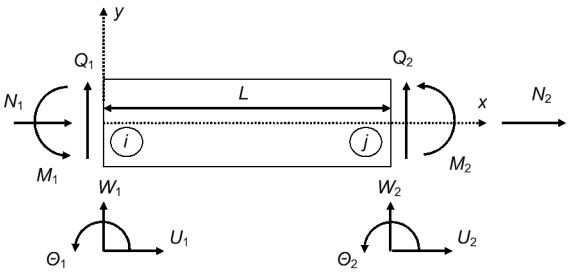

Fig. 3 Nodal displacements and forces

2.3 Natural frequencies and mode shapes of multiple cracked FGM frame

In general, for a given structure that consists of a number (n_e) of FGM beam elements, the total dynamic stiffness matrix for the structure is assembled by

$$\boldsymbol{D}(\omega)=\sum_{e=1}^{n_e}\boldsymbol{T}_e^{-1}\boldsymbol{D}_e(\omega)\boldsymbol{T}_e,\tag{19}$$

where $\boldsymbol{T}_e$ is the matrix of the co-ordinate transform for the eth element. After assembling the total dynamic stiffness matrix with total vector of displacements $\boldsymbol{U}$, free vibration of the structure is described by

$$\boldsymbol{D}(\omega)\boldsymbol{U}=\boldsymbol{0},\tag{20}$$

and the natural frequencies of the structure are computed as positive roots of the equation

$$\det[\boldsymbol{D}(\omega)]=0,\tag{21}$$

and the mode shape corresponding to the natural frequency ω_k is calculated for every element as

$$\phi_k^e(x)=C_k^0\boldsymbol{\Phi}\left(x,\omega_k\right)\begin{bmatrix}\boldsymbol{\Phi}(0,\omega_k)\\ \boldsymbol{\Phi}(L,\omega_k)\end{bmatrix}^{-1}\boldsymbol{T}_e\hat{\boldsymbol{U}}_k,\tag{22}$$

where C_k^0 is an arbitrary constant and $\hat{\boldsymbol{U}}_k$ is the normalized solution of Eq. (20) for a given ω_k.

3 Stationary wavelet transform

The wavelet transform (WT) and discrete wavelet transform (DWT) were proved in (Deng and Wang, 1998; Liew and Wang, 1998; Quek et al., 2001; Douka et al., 2003; Chang and Chen, 2005) to be an efficient tool for structural crack detection. That is because the WT and DWT of a signal enable the revelation of a small change in the signal such as sharp transitions usually caused by a crack in a structure. Despite the success of the DWT-based technique for crack detection in structures, the non-invariance in time/space and noise-sensitivity of DWT are still drawbacks of the technique. To overcome these restrictions, the so-called SWT was introduced (Pesquet et al., 1996) and applied for crack detection in beams (Zhong and Oyadiji, 2007) and frame structures (Ovanesova and Suarez, 2004). The SWT consists of modified approximation $\tilde{A}_{j,k}$ and detailed coefficients $\tilde{D}_{j,k}$ (Zhong and Oyadiji, 2007):

$$\begin{aligned}\tilde{A}_{j,k} &= 2^{-j/2}\int_{-\infty}^{\infty} f(x)\varphi\left(\frac{x-k}{2^j}\right)\mathrm{d}x,\\ \tilde{D}_{j,k} &= 2^{-j/2}\int_{-\infty}^{\infty} f(x)\psi\left(\frac{x-k}{2^j}\right)\mathrm{d}x,\end{aligned} \tag{23}$$

where $\varphi(x)$ is the DWT, $\psi(x)$ is the scaling function, and j and k are integers.

In this study, the SWT from mode shapes of a simple portal frame made of FGM is applied. The detailed coefficients of the mode shapes are examined to detect cracks in the structure.

4 Multiple crack detection by the neural networks

The NNs have been proved to be a reliable technique not only for solving the inverse/optimization problems such as image processing, object recognition, speech recognition, and structural damage identification owing to their capabilities of pattern recognition and classification (Wu et al., 1992; Liu et al., 2002; Yam et al., 2003; Zapico et al., 2003; Mehrjoo et al., 2008; Nematollahi et al., 2012; Aydin and Kisi, 2015; Hakim et al., 2016) but also for direct problems in engineering such as finding solutions of partial differential equations (Anitescu et al., 2019; Guo et al., 2019; Samaniego et al., 2020). They also have noise filtering capabilities that make them more robust in the presence of measurement noise and other uncertainties. The NN-based damage identification is completed with the model that correlates the behavior of a structure, such as modal parameters or response, with damage parameters via a training process. Once the relationship has been established, the trained NN model is capable of detecting damage from the measured quantities.

NN is organized by layers. Each layer is made of nodes which consist of the active function. Data from an input layer is moved to one or several hidden layers where operation processes occur through the connection weights. Then hidden layers connect to an output layer (Fig. 4). The NN used in this study is a multi-layer feed-forward (MLFF) neutral network. It consists of an input, some hidden layers, and an output. Transfer functions of neurons of the hidden and output layers are defined in Eq. (24) using the Tansig function (Nazari and Abolbashari, 2013).

$$f(x) = \frac{2}{1+\exp(-2x)} - 1. \tag{24}$$

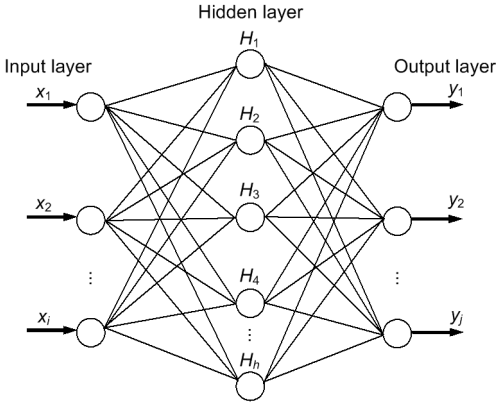

Fig. 4 Diagram of a typical NN architecture

NN has learning rules to adjust connection weights based on input data. Among many learning rules, back-propagation is the best-known one. This is

a supervised process which is operated in each epoch, i.e. each time new data samples go into the network. It contains one forward-stage of neural going in and out of the network, and one backward-stage that adjusts connection weights based on calculation errors to reach the global minimum. As NN is trained to a suitable level, it can be used for analysis of other data, in what is called the test mode. In this mode, the connection weights are constants and the network only works in the forward stage; input data will be processed through trained layers to obtain the desired output values. The back-error propagation (BEP) algorithm is the most widely used learning algorithm for the MLFF neural network. This learning method was proposed by Rumelhart and Mcclelland (1986) in a ground-breaking study originally focused on cognitive computer science. The BEP consists of three stages (Nazari and Abolbashari, 2013). Repeating these three stages led to a value of the error function that will be zero or a constant.

The prediction accuracy of NN is based on mean square error (MSE) which is given by

$$\mathrm{MSE}=\sqrt{\frac{1}{M}\sum_{i=1}^{M}\left(d^{(i)}-y^{(i)}\right)^2}, \tag{25}$$

where $y^{(i)}$ is the network output, $d^{(i)}$ is the desired output, and M is the number of training patterns (input-output pairs).

5 Results and discussion

5.1 Natural frequencies and mode shapes

In this subsection, the natural frequency and mode shapes of a portal frame consisting of three beam members *AB*, *BC*, and *CD* as shown in Fig. 5 are computed and compared to those obtained in previous study (Banerjee and Ananthapuvirajah, 2018). The supports at both points *A* and *D* can be either simply supported (Fig. 5a) or clamped (Fig. 5b). All three members of the portal frame are assumed to have the same rectangular cross-section and a length of 1 m. The width and height of the cross-section are 0.04 m and 0.02 m, respectively. Numerical computation is accomplished in the three following scenarios: (1) *AB* and *CD* are made of isotropic material, *BC* is made of FGM; (2) *AB* and *CD* are made of FGM, *BC* is made of isotropic material; (3) *AB*, *BC*, and *CD* are all made of FGM. The isotropic material considered herein is steel with Young's modulus E_2= 200 GPa and density 7500 kg/m^3. The FGM is composed of steel at the bottom and a ceramic with Young's modulus 380 GPa and density 3960 kg/m^3 on the top. The frequency parameter λ_i computed herein is related to the natural frequency, ω_i, of the structure by $\lambda_i=\omega_i\sqrt{\rho_{\mathrm{b}}AL^4/(E_{\mathrm{b}}I)}$.

The frequency parameter of the first three modes has been computed by the procedure proposed above and compared to that obtained by Banerjee and Ananthapuvirajah (2018) in case of simple support at points *A* and *D* and different power law exponent values *n* (Table 1). Obviously, the discrepancy between the results does not exceed 1.8%. Mode shapes corresponding to the natural frequencies are shown in Fig. 6. Fig. 6 also demonstrates an excellent agreement between numerical results obtained in the present study and Banerjee and Ananthapuvirajah (2018) and validates the usefulness of the DSM developed above for modal analysis of a multiple cracked FGM frame.

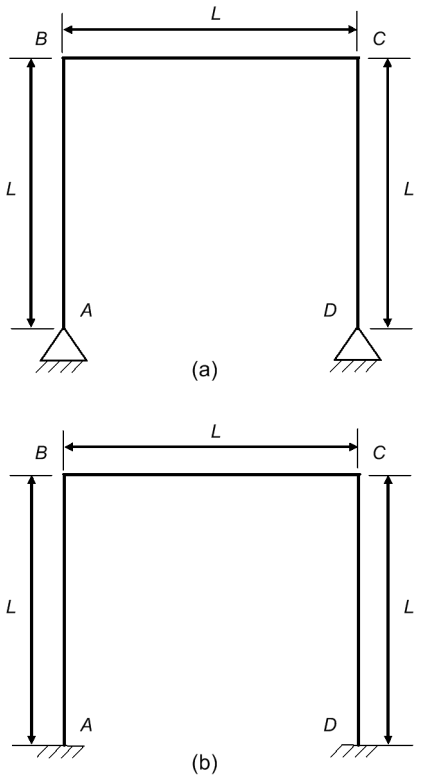

Fig. 5 A portal frame: (a) simply supported; (b) clamped

Table 1 Comparison of frequency parameter computed in present study with that given in reference (Banerjee and Ananthapuvirajah, 2018) for the portal frame

Scenario		*AB*, *CD*: isotropic; *BC*: FGM			*AB*, *CD*: FGM; *BC*: isotropic			*AB*, *CD*, *BC*: FGM		
		λ_1	λ_2	λ_3	λ_1	λ_2	λ_3	λ_1	λ_2	λ_3
n=0.5	Present	1.7031	11.1714	16.4054	1.8361	12.6414	20.2246	2.1912	14.7740	22.2309
	Reference*	1.694	11.083	16.282	1.831	12.617	20.301	2.211	14.906	22.434
n=1.0	Present	1.6424	10.8728	16.0141	1.7446	11.9589	18.7312	1.9802	13.3635	20.1084
	Reference*	1.640	10.848	15.961	1.752	12.025	18.917	2.015	13.583	20.438
n=5.0	Present	1.5389	10.3528	15.3747	1.6004	10.8447	16.5509	1.6876	11.3785	17.1213
	Reference*	1.541	10.375	15.394	1.610	10.921	16.694	1.708	11.518	17.334

* Banerjee and Ananthapuvirajah (2018)

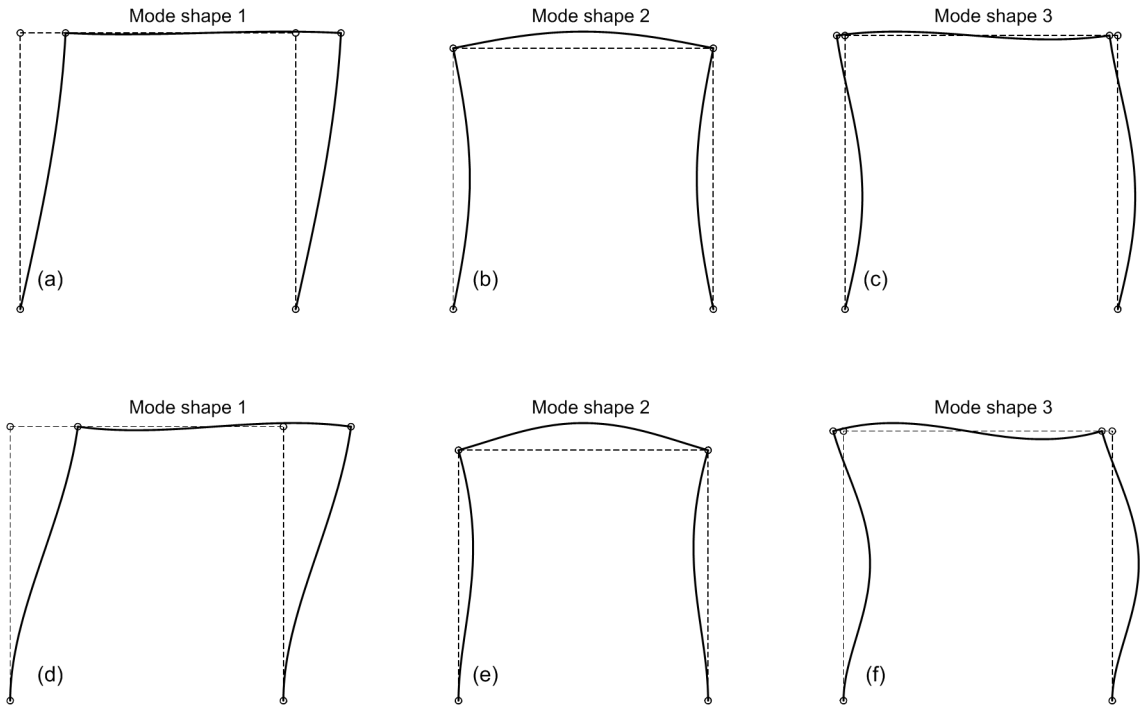

Fig. 6 The first three mode shapes of the portal frame when the points *A* and *D* are simply supported (a)–(c) and clamped (d)–(f). Dashed line: undeformed frame; solid line: mode shape

Figs. 7a–7c show the deviation of the mode shapes from the intact ones computed for the portal frame with two cracks at positions 0.3 m and 0.6 m on the horizontal FGM member *BC* with relative depths of 10%, 20%, and 30%. Figs. 7d–7f present the mode shape deviations in the case of six cracks of equal depth (10%, 20%, 30%) appearing at all three members *AB* (two cracks at 0.2 m and 0.5 m from the support *A*), *BC* (two cracks at 0.3 m and 0.6 m from left node *B*), and *CD* (two cracks at 0.3 m and 0.7 m from the support *D*).

We can find that the mode shapes are all smooth for the frame with intact (uncracked) beam members, but they have a sharp peak deviation at the crack locations because of cracks. Although the peak deviations may not be the maximum variation of the mode shapes themselves, such change in a signal can be easily discriminated by the wavelet analysis. Thus,

the mode shapes of the cracked FGM frame would be analyzed below by using the SWT described above.

5.2 Wavelet analysis of cracked FGM portal frame

Fig. 8 presents the wavelet detail coefficients SWT dB4 of the three mode shapes in the case of two cracks at positions 0.3 m and 0.6 m on the beam *BC* of the FGM portal frame and Fig. 9 shows the wavelet coefficients of the mode shapes for the frame with six cracks. From the two figures, we can find that:

1. Sudden changes in the wavelet detail coefficient are clearly visible at the crack positions for all the shape modes that are examined, while the coefficient is almost unchanged along the uncracked zones. Thus, any crack position can be confidently detected from the wavelet detail coefficient of only one mode shape of the cracked structure. Obviously, crack positions can be identified by the locations where the wavelet coefficient has a sudden peak change.

2. The magnitude of the sudden change in the wavelet coefficient is more clearly shown for a crack of larger depth. This recalls the well-known fact that more severe cracks are easier to detect than the small ones and it is true also in crack detection in an FGM frame using wavelet transform of mode shapes.

3. However, multiple cracks of the same depth located at different positions on the frame lead to different changes in the wavelet detail coefficient of mode shape. This implies that the change in magnitude of the wavelet detail coefficient is dependent not only on the crack depth but also on its position.

4. Moreover, increasing the density of the grid used for computing or measuring the mode shapes leads to a significant increase of change in the wavelet coefficient, while the effect of crack depth is almost independent of the grid.

5.3 Effect of noise on wavelet detail coefficient

To assess the effect of unavoidable noise on measurements of mode shapes, in this subsection the wavelet detail coefficient is computed with mode shapes under noisy conditions. Thus, we consider the simply supported FGM portal frame (Fig. 5a) with two cracks of depth 30% at positions 0.3 m and 0.6 m on the beam *BC*. Input signals are mode shapes of the cracked FGM portal frame added by noise of different

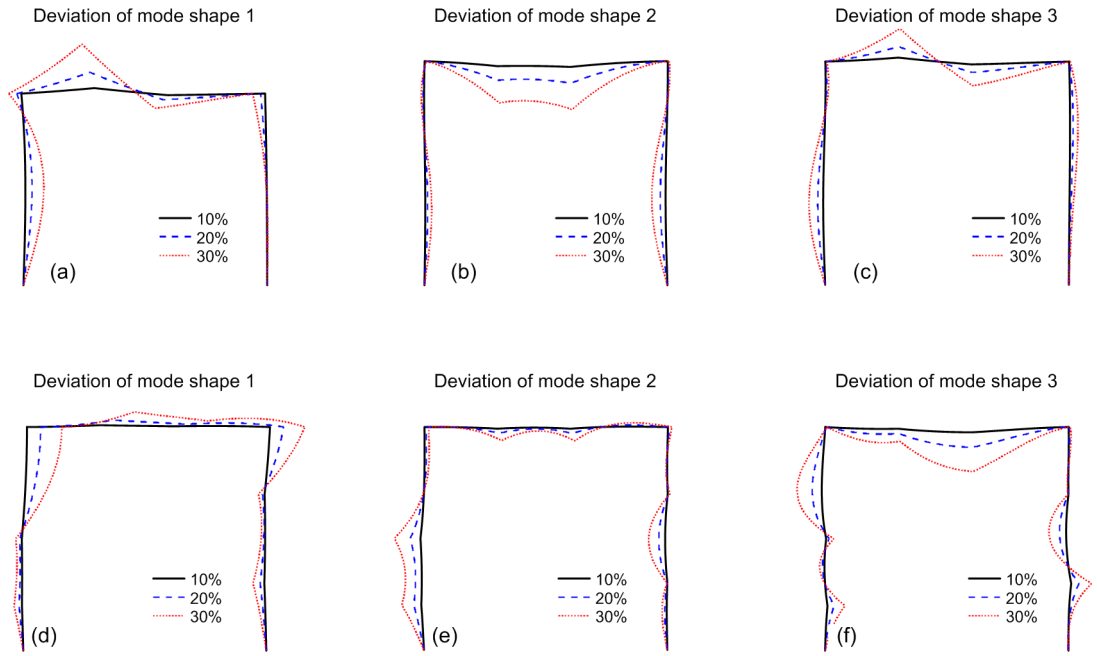

Fig. 7 Deviation of the first three mode shapes of the simply supported FGM portal frame with two cracks on *BC* (a)–(c) or six cracks on *AB*, *CD*, and *BC* (d)–(f) of relative depths of 10%, 20%, and 30%

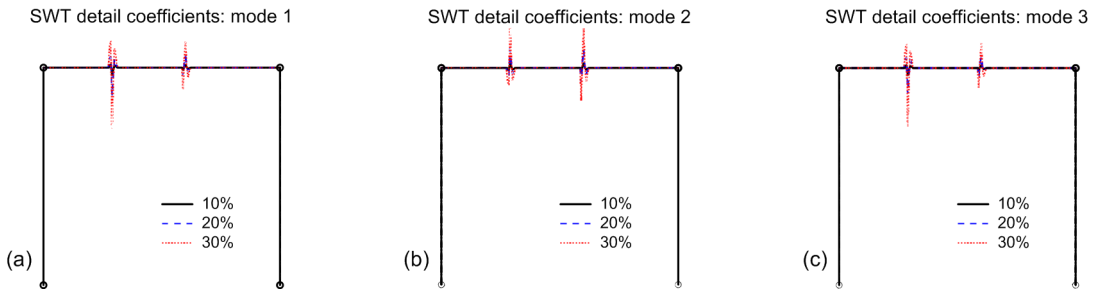

Fig. 8 Wavelet detail coefficients of the FGM portal frame using the first (a), the second (b), and the third (c) mode shapes when the frame has two cracks on *BC*

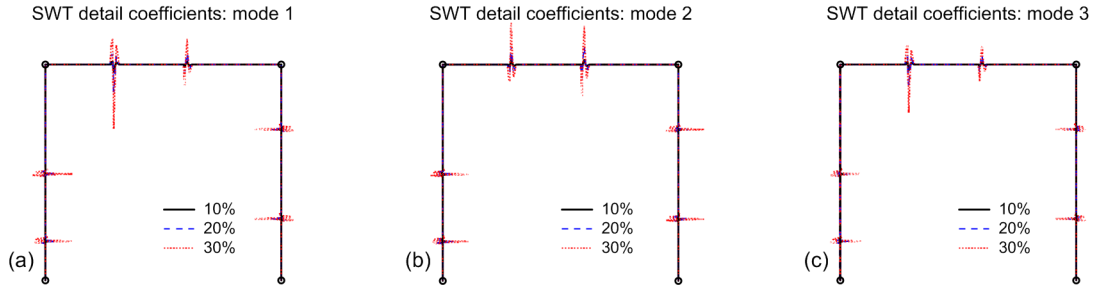

Fig. 9 Wavelet detail coefficients of the FGM portal frame using the first (a), the second (b), and the third (c) mode shapes when the frame has six cracks on *AB*, *CD*, and *BC*

signal-noise ratio (SNR) levels of 95 dB, 100 dB, and 105 dB. The computed wavelet detail coefficients SWT dB4 of the noisy mode shapes are shown in Fig. 10 for the first three modes.

The obvious effect of noise on the wavelet coefficient can be seen. However, sudden changes in the coefficient caused by cracks are still clearly visible at all the noise levels. This demonstrates again the detectability of cracks in an FGM frame even from noisy measured mode shapes.

5.4 Crack identification from SWT detail coefficient and NN

In this subsection, a procedure is proposed to identify multiple cracks in an FGM frame using SWT detail coefficients of mode shapes in combination with the NN technique. As shown above, crack locations are easily detected from wavelet detail coefficients computed for any mode shape. Thus, supposing that crack locations are known and we need to predict the depth of the localized cracks from the wavelet coefficient with the NN technique. Fig. 11 presents the flowchart of the crack identification in FGM using SWT and ANN.

Two case studies are accomplished for the above FGM portal frame (Fig. 5a) as follows.

Firstly, the frame with two cracks at 0.3 m and 0.6 m on the beam *BC* is considered. Assuming that the SWT dB4 of fundamental mode shape has been given, an NN with input data of the SWT dB4 detail coefficient is created for crack depth prediction. Namely, MLFF NNs with an input layer consisting of 100 neurons (corresponding to the number of SWT detail coefficients), 10 hidden layers, and an output layer consisting of two neurons (corresponding to the number of prediction crack depths) are generated. The SWT dB4 detail coefficients of the fundamental mode shape of the FGM portal frame in 64 different crack depth scenarios are applied to NNs as the input of the networks. Training the NNs is done by using the BEP algorithm with 1000 epochs. The BEP training procedure for depth prediction of the two cracks is

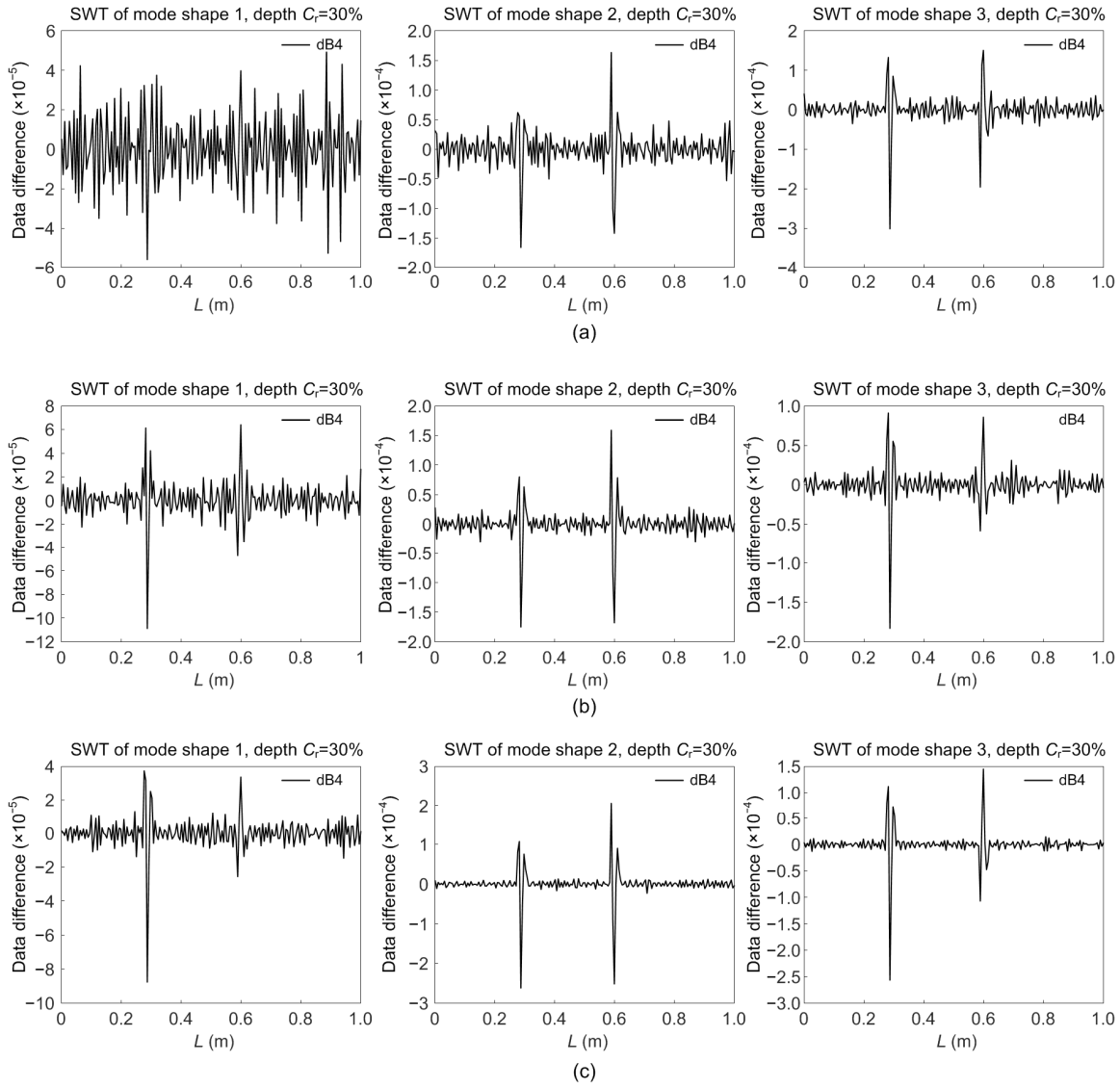

Fig. 10 Wavelet detail coefficients of the first (left), the second (middle), and the third (right) mode shapes with relative depths of 30% under different SNR levels: (a) 95 dB; (b) 100 dB; (c) 105 dB

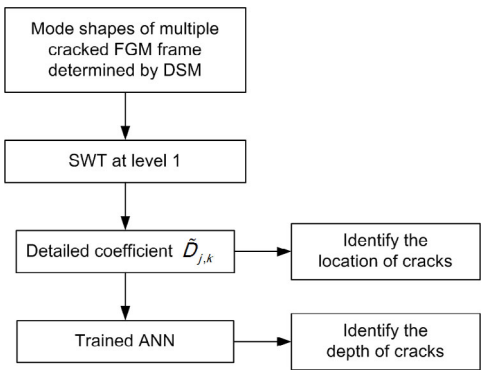

Fig. 11 Flowchart of the crack identification in FGM frames using SWT and ANN

plotted in Fig. 12. The trained NNs were used for predicting depths of cracks (in four different cases) as tabulated in Table 2 corresponding to different SNR noise levels of 95 dB, 100 dB, and 105 dB, respectively.

Secondly, the frame has two cracks at column *AB* and two cracks at the beam *BC*. MLFF NNs with an input layer consisting of 200 neurons (corresponding to the number of SWT detail coefficients of the column *AB* and beam *BC*), 10 hidden layers, and an output layer consisting of four neurons (corresponding to the number of prediction crack depths)

are created. The SWT dB4 detail coefficients of the fundamental mode shape of the FGM portal frame in 4096 different crack depth conditions are applied to NNs as the input of the networks. Training the NNs is done by using the BEP algorithm with epochs. BEP training procedure for prediction of depths of the four cracks is plotted in Fig. 13. The trained NNs were used to predict depths of cracks in four different cases as tabulated in Table 3 without noise for simplification.

As can be seen from Tables 2 and 3, errors in prediction of two cracks with noisy wavelet detail coefficient and four cracks without noisy wavelet detail coefficient are less than 5%. This is a good result in prediction of multiple crack depths.

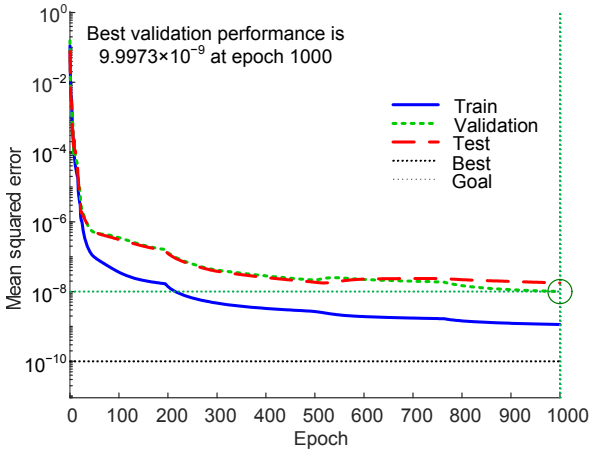

Fig. 12 Mean squared error of the NN training procedure for depth prediction of the two cracks

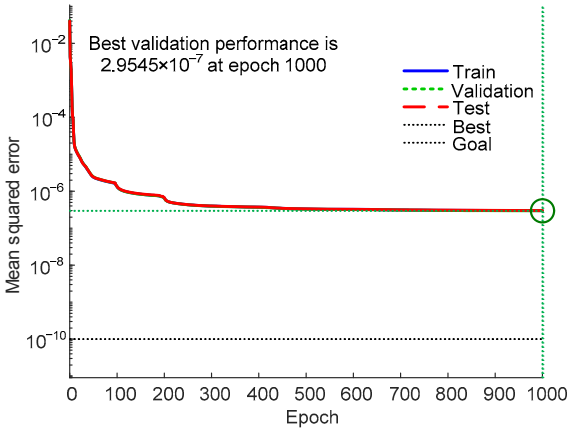

Fig. 13 Mean squared error of the NN training procedure for depth prediction of the four cracks

6 Conclusions

This study allows one to make the following concluding remarks:

1. The dynamic stiffness model developed herein for multiple cracked frames made of FGM provides an exact and powerful tool for modal analysis of multiple cracked FGM structures in an arbitrary high frequency band.

2. It was demonstrated that the SWT as a filtered wavelet transform applied for mode shapes is an efficient technique in localizing cracks in frame FGM structures. The numerical example also shows that for accurate localization of cracks it is enough to use only the fundamental mode shape.

Table 3 Prediction of four crack depths using NN

Case number	Crack	Actual depth (cm)	Prediction depth (cm)	Error (%)
1	1st	0.2	0.2068	3.40
	2nd	0.3	0.2886	−3.80
	3rd	0.3	0.2917	−2.77
	4th	0.4	0.4159	3.98
2	1st	0.3	0.2913	−2.90
	2nd	0.2	0.1898	−5.10
	3rd	0.4	0.3939	−1.53
	4th	0.3	0.3279	9.30

Table 2 Prediction of two crack depths using NN

Case number	Crack	Actual depth (cm)	SNR=95 dB		SNR=100 dB		SNR=105 dB	
			Prediction depth (cm)	Error (%)	Prediction depth (cm)	Error (%)	Prediction depth (cm)	Error (%)
1	1st	0.2	0.1927	−3.65	0.1955	−2.25	0.1991	−0.45
	2nd	0.3	0.3019	0.63	0.3010	0.33	0.3001	0.03
2	1st	0.3	0.3112	3.73	0.3069	2.30	0.3013	0.43
	2nd	0.3	0.3053	1.77	0.3030	1.00	0.3004	0.13
3	1st	0.2	0.1924	−3.80	0.1952	−2.40	0.1990	−0.50
	2nd	0.2	0.1983	−0.85	0.1989	−0.55	0.1997	−0.15
4	1st	0.3	0.3129	4.30	0.3080	2.67	0.3016	0.53
	2nd	0.4	0.4185	4.63	0.4111	2.78	0.4019	0.48

3. The NN technique in combination with the SWT of the mode shape is shown to be very effective for accurately assessing crack depth in composite structures such as one made of FGM, even with noisy measured mode shapes.

4. The integrated procedure proposed for multiple cracked identification of FGM frame in this study is useful in the case of a limited amount of measured data not only of the mode shape but also of static or dynamic deflection of the structures.

Contributors

Tran Van LIEN designed the research. Ngo Trong DUC processed the corresponding data. Tran Van LIEN wrote the first draft of the manuscript. Nguyen Tien KHIEM helped to organize the manuscript. Tran Van LIEN revised and edited the final version.

Conflict of interest

Nguyen Tien KHIEM, Tran Van LIEN, and Ngo Trong DUC declare that they have no conflict of interest.

References

Abolbashari MH, Nazari F, Rad JS, 2014. A multi-crack effects analysis and crack identification in functionally graded beams using particle swarm optimization algorithm and artificial neural network. *Structural Engineering and Mechanics*, 51(2):299-313. https://doi.org/10.12989/sem.2014.51.2.299

Akbaş ŞD, 2013. Free vibration characteristics of edge cracked functionally graded beams by using finite element method. *International Journal of Engineering Trends and Technology*, 4(10):4590-4597.

Anitescu C, Atroshchenko E, Alajlan N, et al., 2019. Artificial neural network methods for the solution of second order boundary value problems. *Computers, Materials & Continua*, 59(1):345-359. https://doi.org/10.32604/cmc.2019.06641

Aydin K, 2013. Free vibration of functionally graded beams with arbitrary number of surface cracks. *European Journal of Mechanics-A/Solids*, 42:112-124. https://doi.org/10.1016/j.euromechsol.2013.05.002

Aydin K, Kisi O, 2015. Damage diagnosis in beam-like structures by artificial neural networks. *Journal of Civil Engineering and Management*, 21(5):591-604. https://doi.org/10.3846/13923730.2014.890663

Banerjee A, Panigrahi B, Pohit G, 2016. Crack modelling and detection in Timoshenko FGM beam under transverse vibration using frequency contour and response surface model with GA. *Nondestructive Testing and Evaluation*, 31(2):142-164. https://doi.org/10.1080/10589759.2015.1071812

Banerjee JR, Ananthapuvirajah A, 2018. Free vibration of functionally graded beams and frameworks using the dynamic stiffness method. *Journal of Sound and Vibration*, 422:34-47. https://doi.org/10.1016/j.jsv.2018.02.010

Caddemi S, Caliò I, 2013. The exact explicit dynamic stiffness matrix of multi-cracked Euler–Bernoulli beam and applications to damaged frame structures. *Journal of Sound and Vibration*, 332(12):3049-3063. https://doi.org/10.1016/j.jsv.2013.01.003

Caddemi S, Caliò I, Cannizzaro F, et al., 2018. A procedure for the identification of multiple cracks on beams and frames by static measurements. *Structural Control and Health Monitoring*, 25(8):e2194. https://doi.org/10.1002/stc.2194

Chakraverty S, Pradhan KK, 2016. Vibration of Functionally Graded Beams and Plates. Academic Press, London, UK.

Chang CC, Chen LW, 2005. Detection of the location and size of cracks in the multiple cracked beam by spatial wavelet based approach. *Mechanical Systems and Signal Processing*, 19(1):139-155. https://doi.org/10.1016/j.ymssp.2003.11.001

Deng XM, Wang Q, 1998. Crack detection using spatial measurements and wavelet analysis. *International Journal of Fracture*, 91(2):L23-L28.

Douka E, Loutridis S, Trochidis A, 2003. Crack identification in beams using wavelet analysis. *International Journal of Solids and Structures*, 40(13-14):3557-3569. https://doi.org/10.1016/S0020-7683(03)00147-1

Eftekhari M, Eftekhari M, Hosseini M, 2013. Crack detection in functionally graded beams using conjugate gradient method. *International Journal of Engineering-Transactions C: Aspects*, 27(3):367-374.

Elishakoff I, Pentaras D, Gentilini C, 2016. Mechanics of Functionally Graded Material Structures. World Scientific, Singapore. https://doi.org/10.1142/9505

Eltaher MA, Alshorbagy AE, Mahmoud FF, 2013. Determination of neutral axis position and its effect on natural frequencies of functionally graded macro/nanobeams. *Composite Structures*, 99:193-201. https://doi.org/10.1016/j.compstruct.2012.11.039

Erdogan F, Wu BH, 1997. The surface crack problem for a plate with functionally graded properties. *Journal of Applied Mechanics*, 64(3):449-456. https://doi.org/10.1115/1.2788914

Gu P, Asaro RJ, 1997. Cracks in functionally graded materials. *International Journal of Solids and Structures*, 34(1):1-17. https://doi.org/10.1016/0020-7683(95)00289-8

Guo HW, Zhuang XY, Rabczuk T, 2019. A deep collocation method for the bending analysis of kirchhoff plate. *Computers, Materials & Continua*, 59(2):433-456. https://doi.org/10.32604/cmc.2019.06660

Hakim SJS, Razak HA, Ravanfar SA, 2016. Ensemble neural networks for structural damage identification using modal data. *International Journal of Damage Mechanics*, 25(3):400-430.

https://doi.org/10.1177/1056789515598639

Jin ZH, Batra RC, 1996. Some basic fracture mechanics concepts in functionally graded materials. *Journal of the Mechanics and Physics of Solids*, 44(8):1221-1235. https://doi.org/10.1016/0022-5096(96)00041-5

Ke LL, Yang J, Kitipornchai S, et al., 2009. Flexural vibration and elastic buckling of a cracked Timoshenko beam made of functionally graded materials. *Mechanics of Advanced Materials and Structures*, 16(6):488-502. https://doi.org/10.1080/15376490902781175

Khiem NT, 2006. Crack detection for structure based on the dynamic stiffness model and the inverse problem of vibration. *Inverse Problems in Science and Engineering*, 14(1):85-96. https://doi.org/10.1080/17415970500272908

Khiem NT, Huyen NN, 2016. Uncoupled vibrations in functionally graded Timoshenko beam. *Vietnam Journal of Science and Technology*, 54(6):785-796. https://doi.org/10.15625/0866-708X/54/6/7719

Khiem NT, Huyen NN, 2017. A method for crack identification in functionally graded Timoshenko beam. *Nondestructive Testing and Evaluation*, 32(3):319-341. https://doi.org/10.1080/10589759.2016.1226304

Khiem NT, Huyen NN, Long NT, 2017. Vibration of cracked Timoshenko beam made of functionally graded material. *In*: Harvie JM, Baqersad J (Eds.), Shock & Vibration, Aircraft/Aerospace, Energy Harvesting, Acoustics & Optics, Volume 9. Springer, Cham, Germany, p.133-143. https://doi.org/10.1007/978-3-319-54735-0_15

Kitipornchai S, Ke LL, Yang J, et al., 2009. Nonlinear vibration of edge cracked functionally graded Timoshenko beams. *Journal of Sound and Vibration*, 324(3-5):962-982. https://doi.org/10.1016/j.jsv.2009.02.023

Larbi LO, Kaci A, Houari MSA, et al., 2013. An efficient shear deformation beam theory based on neutral surface position for bending and free vibration of functionally graded beams[#]. *Mechanics Based Design of Structures and Machines*, 41(4):421-433. https://doi.org/10.1080/15397734.2013.763713

Liew KM, Wang Q, 1998. Application of wavelet theory for crack identification in structures. *Journal of Engineering Mechanics*, 124(2):152-157. https://doi.org/10.1061/(asce)0733-9399(1998)124:2(152)

Lien VT, Duc NT, 2019. Crack identification in multiple cracked beams made of functionally graded material by using stationary wavelet transform of mode shapes. *Vietnam Journal of Mechanics*, 41(2):105-126. https://doi.org/10.15625/0866-7136/12835

Lien VT, Duc NT, Hung DT, 2019a. Crack identification in FGM multi-span beams using neural network and stationary wavelet transform of mode shapes and dynamic deflections. Proceedings of the National Science Conference Engineering Mechanics (in Vietnamese).

Lien VT, Duc NT, Khiem NT, 2019b. Free and forced vibration analysis of multiple cracked FGM multi span continuous beams using dynamic stiffness method. *Latin American Journal of Solids and Structures*, 16(2):e157. https://doi.org/10.1590/1679-78255242

Liu SW, Huang JH, Sung JC, et al., 2002. Detection of cracks using neural networks and computational mechanics. *Computer Methods in Applied Mechanics and Engineering*, 191(25-26):2831-2845. https://doi.org/10.1016/S0045-7825(02)00221-9

Matbuly MS, Ragb O, Nassar M, 2009. Natural frequencies of a functionally graded cracked beam using the differential quadrature method. *Applied Mathematics and Computation*, 215(6):2307-2316. https://doi.org/10.1016/j.amc.2009.08.026

Mehrjoo M, Khaji N, Moharrami H, et al., 2008. Damage detection of truss bridge joints using Artificial Neural Networks. *Expert Systems with Applications*, 35(3):1122-1131. https://doi.org/10.1016/j.eswa.2007.08.008

Nanthakumar SS, Lahmer T, Zhuang X, et al., 2016. Detection of material interfaces using a regularized level set method in piezoelectric structures. *Inverse Problems in Science and Engineering*, 24(1):153-176. https://doi.org/10.1080/17415977.2015.1017485

Nazari F, Abolbashari MH, 2013. Double cracks identification in functionally graded beams using artificial neural network. *Journal of Solid Mechanics*, 5(1):14-21.

Nematollahi MA, Farid M, Hematiyan MR, et al., 2012. Crack detection in beam-like structures using a wavelet-based neural network. *Proceedings of the Institution of Mechanical Engineers, Part G: Journal of Aerospace Engineering*, 226(10):1243-1254. https://doi.org/10.1177/0954410011421709

Ovanesova AV, Suarez LE, 2004. Applications of wavelet transforms to damage detection in frame structures. *Engineering Structures*, 26(1):39-49. https://doi.org/10.1016/j.engstruct.2003.08.009

Pan FY, Li WJ, Wang BL, et al., 2009. Viscoelastic fracture of multiple cracks in functionally graded materials. *Computer Methods in Applied Mechanics and Engineering*, 198(33-36):2643-2649. https://doi.org/10.1016/j.cma.2009.03.005

Panigrahi B, Pohit G, 2018. Study of non-linear dynamic behavior of open cracked functionally graded Timoshenko beam under forced excitation using harmonic balance method in conjunction with an iterative technique. *Applied Mathematical Modelling*, 57:248-267. https://doi.org/10.1016/j.apm.2018.01.022

Pesquet JC, Krim H, Carfantan H, 1996. Time-invariant orthonormal wavelet representations. *IEEE Transactions on Signal Processing*, 44(8):1964-1970. https://doi.org/10.1109/78.533717

Quek ST, Wang Q, Zhang L, et al., 2001. Sensitivity analysis of crack detection in beams by wavelet technique. *International Journal of Mechanical Sciences*, 43(12):2899-2910.

https://doi.org/10.1016/S0020-7403(01)00064-9

Rumelhart DE, McClelland JL, 1987. Parallel Distributed Processing: Explorations in the Microstructure of Cognition: Foundations. MIT Press, USA.

Samaniego E, Anitescu C, Goswami S, et al., 2020. An energy approach to the solution of partial differential equations in computational mechanics via machine learning: concepts, implementation and applications. *Computer Methods in Applied Mechanics and Engineering*, 362:112790. https://doi.org/10.1016/j.cma.2019.112790

Sherafatnia K, Farrahi GH, Faghidian SA, 2013. Analytic approach to free vibration and buckling analysis of functionally graded beams with edge cracks using four engineering beam theories. *International Journal of Engineering-Transactions C: Aspects*, 27(6):979-990. https://doi.org/10.5829/idosi.ije.2014.27.06c.17

Su H, Banerjee JR, 2015. Development of dynamic stiffness method for free vibration of functionally graded Timoshenko beams. *Computers & Structures*, 147:107-116. https://doi.org/10.1016/j.compstruc.2014.10.001

Wei D, Liu YH, Xiang ZH, 2012. An analytical method for free vibration analysis of functionally graded beams with edge cracks. *Journal of Sound and Vibration*, 331(7): 1686-1700. https://doi.org/10.1016/j.jsv.2011.11.020

Wu X, Ghaboussi J, Garrett Jr JH, 1992. Use of neural networks in detection of structural damage. *Computers & Structures*, 42(4):649-659. https://doi.org/10.1016/0045-7949(92)90132-J

Yam LH, Yan YJ, Jiang JS, 2003. Vibration-based damage detection for composite structures using wavelet transform and neural network identification. *Composite Structures*, 60(4):403-412. https://doi.org/10.1016/S0263-8223(03)00023-0

Yan T, Kitipornchai S, Yang J, et al., 2011. Dynamic behaviour of edge-cracked shear deformable functionally graded beams on an elastic foundation under a moving load. *Composite Structures*, 93(11):2992-3001. https://doi.org/10.1016/j.compstruct.2011.05.003

Yang J, Chen Y, 2008. Free vibration and buckling analyses of functionally graded beams with edge cracks. *Composite Structures*, 83(1):48-60. https://doi.org/10.1016/j.compstruct.2007.03.006

Yang J, Chen Y, Xiang Y, et al., 2008. Free and forced vibration of cracked inhomogeneous beams under an axial force and a moving load. *Journal of Sound and Vibration*, 312(1-2):166-181. https://doi.org/10.1016/j.jsv.2007.10.034

Yu ZG, Chu FL, 2009. Identification of crack in functionally graded material beams using the *p*-version of finite element method. *Journal of Sound and Vibration*, 325(1-2):69-84. https://doi.org/10.1016/j.jsv.2009.03.010

Zapico JL, González MP, Worden K, 2003. Damage assessment using neural networks. *Mechanical Systems and Signal Processing*, 17(1):119-125. https://doi.org/10.1006/mssp.2002.1547

Zhong SC, Oyadiji SO, 2007. Crack detection in simply supported beams without baseline modal parameters by stationary wavelet transform. *Mechanical Systems and Signal Processing*, 21(4):1853-1884. https://doi.org/10.1016/j.ymssp.2006.07.007

Zhu LF, Ke LL, Zhu XQ, et al., 2019. Crack identification of functionally graded beams using continuous wavelet transform. *Composite Structures*, 210:473-485. https://doi.org/10.1016/j.compstruct.2018.11.042